Document downloaded from:

http://hdl.handle.net/10251/155248

This paper must be cited as:

Rodríguez-Fernández, A.; Atienzar Corvillo, PE.; Martínez, C.; Román-Leshkov, Y.; Moliner Marin, M. (2019). Ge-Based Hybrid Composites from Ge-Rich Zeolites as Highly Conductive and Stable Electronic Materials. Chemistry of Materials. 31(18):7723-7731. https://doi.org/10.1021/acs.chemmater.9b02696

The final publication is available at

https://doi.org/10.1021/acs.chemmater.9b02696

Copyright American Chemical Society

Additional Information

This document is the Accepted Manuscript version of a Published Work that appeared in final form in Chemistry of Materials, copyright © American Chemical Society after peer review and technical editing by the publisher. To access the final edited and published work see https://doi.org/10.1021/acs.chemmater.9b02696.

Ge-based hybrid composites from Ge-rich zeolites as highly conductive and stable electronic materials

Aída Rodríguez-Fernández,[1] Pedro Atienzar,[1] Cristina Martínez,[1] Yuriy Román-Leshkov,[2] Manuel Moliner*[1]

[1] Instituto de Tecnología Química, Universitat Politècnica de València-Consejo Superior de Investigaciones Científicas, Avenida de los Naranjos s/n, 46022 València, Spain

[2] Department of Chemical Engineering, Massachusetts Institute of Technology, 77 Massachusetts Ave, Cambridge, MA 02139, United States

*Corresponding author: E-mail address: mmoliner@itq.upv.es

Abstract

Ge-containing zeolites were used as precursors for the synthesis of highly conductive and stable hybrid electronic materials by post-synthetic thermal treatment of the crystals in the presence of an olefin. Treating the as-prepared Ge-zeolites in 1-butene at 700°C formed a graphitic matrix within and outside the crystals due to the thermal degradation of the OSDA inside of the pores and the polymerization of the olefin. Importantly, these conditions forced Ge out of the framework, leading to the collapse of the crystalline structure and subsequent formation of metallic Ge nanoparticles distributed either as small, well-dispersed nanoparticles within the silica matrix or larger carbon-coated core-shell Ge@C nanoparticles on the external surface of the carbon-silica composite. Varying the zeolite topology influenced the size of the Ge@C nanoparticles, with those obtained using the multipore zeolite ITQ-22 (IWW, 12x10x8-rings) featuring smaller sizes (30-60 nm) than those obtained with the large-pore zeolite ITQ-33 (ITT, 18x10x10-rings) (80-120 nm), were the lack of diffusional limitations increased metal sintering rates. The zeolite topology also influenced the final carbon-content and dispersion of the Ge nanoparticles. The best performing Ge-based hybrid material was obtained by thermal treatment of ITQ-22 (Si/Ge=4) at 700°C in 1-butene presents. Unlike Ge-free hybrid controls, an ITQ-22 (Si/Ge=4) sample treated at 700°C in 1-butene showed a conductivity value of ~2 S/m (measured at 1 V), which is in the range of a commercially available graphene. The simple methodology presented here is an alternative route for the efficient preparation of highly stable Ge-based hybrid composites with excellent conductivity for potential use as high-capacity electrodes.

1.- Introduction

In light of the electronics revolution that our society has experienced in the last 20 years with a continuous development of information and communication technologies, many research efforts have been devoted to the design of more efficient, durable, and inexpensive electronic materials.[1-2] The most studied electronic materials are, in general, based on metals, polymers, ceramics, graphenes, and/or composites.[2]

In particular, germanium-based electronic materials have received significant attention because Ge presents outstanding electron and hole mobilities, exemplified, for instance, by an electrical conductivity that is 10^4 times larger compared to that of silicon.[3-4] However, the use of metallic Ge in electronic devices has several drawbacks, including high raw material costs and low stability caused by facile oxidation.[5-6] To circumvent these limitations, efficient synthesis methods have to be developed not only to maximize Ge utilization, but also to adequately protect its external surface to impede undesired oxidation and/or metal sintering.

State-of-the-art strategies to address these challenges include nanostructuring Ge crystals into nanoparticles [7-8] or nanowires (NW),[3-4, 9] as well as their dispersion on large surface supports,[10-13] or their encapsulation within porous matrices.[14-15] The controlled synthesis of Ge nanoparticles with sizes below 50 nm is important to enhance their electronic performance in different applications. For example, when used as electrodes in lithium ion batteries, small Ge particles can alleviate the physical strains associated to the Li uptake/release.[7-8, 16] Unfortunately, the agglomeration of the very small Ge nanoparticles under operation conditions is a serious problem that severely compromises their overall electronic capacity, thus hindering their performance in these devices.[13, 17]

The synthesis of Ge@C core-shell particles or the encapsulation Ge nanoparticles into 3-D interconnected graphene networks have been proposed as efficient approaches to prevent undesired agglomeration.[13, 15] Notably, the presence of aromatic C-species in the hybrid Ge@C composites can enhance chemical properties, reduce metal sintering, and offer superior electron transport and electrical contact between the metal nanoparticles.[18] The synthesis of these materials typically involves the reduction of a previously-deposited Ge precursor with hydrogen and/or inert gases (i.e. N_2 or Ar) at high temperatures (above 600°C)[8, 15, 19], which does not allow the proper control of particle size or degree of encapsulation/dispersion in the final Ge@C composite.

Here, we demonstrate that crystalline Ge-containing zeolites are ideal precursors to synthesize Ge-based hybrid composites with outstanding conductivity and stability. The use of Ge-rich zeolites as precursors has many advantages. First, the wide range of accessible Si/Ge ratios coupled with the labile nature of the tetrahedrally-coordinated Ge atoms in the zeolite framework,[20-22] allows the controlled release of targeted Ge amounts by simple post-synthetic treatments. Second, the microporous topology of the zeolite,[23] automatically confines these extra-framework Ge species without the need of additional encapsulation protocols. Third, the presence of organic molecules used as organic structure directing agents (OSDAs) in the pores of the as-prepared Ge-rich zeolites,[24] can be exploited to prepare a homogeneous inorganic-organic conductive matrix composites containing well-dispersed polycyclic aromatic carbons that can be further complemented by post-synthetic thermal treatments in presence of light olefins.[25] Accordingly, the preselection of zeolite pore topology and initial Ge content can be used to control the distribution of extra-framework Ge particles, both in terms of encapsulation and particle size.

We investigated the electrical properties of Ge-based hybrid composites obtained from two Ge-rich zeolites, namely ITQ-22 (IWW, 12x10x8-rings) [26] and ITQ-33 (ITT, 18x10x10-rings)],[27-28] with Si/Ge contents ranging from 2 to 4, that were subjected to different post-synthetic thermal treatments. The hybrid composite obtained from IWW zeolite with a Si/Ge ratio of ~4 showed a dual distribution of Ge nanoparticles of ~5 nm encapsulated within the silica matrix and core-shell Ge@C nanoparticles of ~30-60 nm located on the external surface of the composite. It featured outstanding conductivity compared to commercially-available graphenes and related C-free and/or Ge-free hybrid composites. Our simple methodology combined with the excellent electrical and chemical properties observed for these Ge-containing composites paves the way for their evaluation as durable, high-capacity electrode materials in diverse devices, including lithium ion batteries.

2.- Experimental

2.1.- Zeolite synthesis

2.1.1.- ITQ-22 with Si/Ge ~ 2 and 4 (IWW-2 and IWW-4)

The ITQ-22 zeolites were synthesized according to synthesis procedures described in the literature using hexamethonium as OSDA.[28] The theoretical molar ratios of the gels were the following: Si/Ge = 2 and 4; B/(Si+Ge) = 0.05; OH/(Si+Ge) = 0.1; OSDA/(Si+Ge) = 0.25; H_2O/(Si+Ge) = 20. The final gels

were heated at 175°C in Teflon-lined stainless steel autoclaves for 7 days, and the resultant solids were filtered, washed, and dried at 100°C.

2.1.2.- ITQ-33 with Si/Ge ~ 2 (ITT-2)

The ITQ-33 zeolite was synthesized according to the synthesis procedure described in the literature using hexamethonium as OSDA.[28] The theoretical molar ratios of the gel were the following: Si/Ge = 2; Al/(Si+Ge) = 0.05; OSDA/(Si+Ge) = 0.25; F/(Si+Ge) = 0.3; H_2O/(Si+Ge) = 2. The final gel was heated at 175°C in a Teflon lined stainless steel autoclave for 1 day, and the resultant solids were filtered, washed, and dried at 100°C.

2.1.3.- Silicalite (MFI)

The synthesis of the silicalite zeolite (MFI) was carried out as follows: 2 g of tetraethylorthosilicate (TEOS) was mixed with 2.3 g of an aqueous solution of tetrapropylammonium hydroxide (TPAOH, 25%wt, Across) and 5 g of water. The mixture was stirred overnight to favor the hydrolysis of TEOS and, afterwards, the evaporation of ethanol and water was controlled until reaching the desired gel concentration. The final gel composition was: 1 SiO_2 : 0.3 TPAOH : 15 H_2O. The gel was loaded into a Teflon-lined stainless steel autoclave, aged for 12 h at 80°C, followed by hydrothermal synthesis for 72 h at 175°C. The resultant solids were filtered, washed, and dried at 100°C.

2.1.4.- Ge-containing graphene materials

For comparison purposes, a Ge/Graphene and a Ge-SiO_2/Graphene have been prepared. For the preparation of Ge/Graphene, 49.2 mg of GeO_2 (Sigma-Aldrich) has been physically mixed with 180.8 mg of graphene (Strem Chemicals), followed by a reduction with H_2 at 700°C for 2 hours. For the preparation of Ge-SiO_2/Graphene, 74.8 mg of GeO_2 (Sigma-Aldrich) has been physically mixed with 229.9 mg of SiO_2 (Aerosil) and 45.3 mg of graphene (Strem Chemicals), followed by a reduction with H_2 at 700°C for 2 hours.

2.1.5.- Post-synthetic treatments

- *Treatments with N_2*: 0.3 g of the as-prepared zeolite was heated at 2°C/min to the desired temperature (580 or 700°C) under a N_2 flow of ~ 100 ml/min, and maintained for 6 h. The sample was cooled down under a flow of N_2.

- *Treatments with $C_4^=$*: 0.3 g of the as-prepared zeolite was first heated at 2°C/min to 80°C under a N_2 flow of ~ 100 ml/min, and maintained at this temperature for 6 h. Then, the temperature was increased to 150°C in N_2 at 2°C/min, and maintained for 2 h. Next, the temperature was increased to the desired value (580 or 700°C) in N_2 at 2°C/min, and once this temperature was reached, the N_2 flow was kept for 2 hours. Finally, a gas mixture formed by 160 ml/min of N_2 and 4 ml/min of butene was passed through the sample at the desired temperature (580 or 700°C) for 4 h. The sample was cooled down under a flow of N_2.

2.2.- Characterization

Powder X-ray diffraction (PXRD) measurements were performed with a multisample Philips X'Pert diffractometer equipped with a graphite monochromator, operating at 40 kV and 35 mA, and using Cu Kα radiation (λ = 0,1542 nm).

Chemical analyses were carried out in a Varian 715-ES ICP-Optical Emission spectrometer, after solid dissolution in HNO_3/HCl/HF aqueous solution. Elemental analyses were performed by combustion analysis using a Eurovector EA 3000 CHNS analyzer.

The morphology of the samples was studied by field emission scanning electron microscopy (FESEM) using a ZEISS Ultra-55 microscope and by field emission transmission electron microscopy (TEM) using a JEM 2100F microscope.

Raman spectra were recorded at ambient temperature with 514 nm excitation on a Renishaw In Via Raman spectrometer equipped with a CCD detector.

2.3.- Conductivity measurements

All the conductivity measurements were performed in a home-made system using a Keithley 2601 sourcemeter connected to a PC using LabTracer software that controls the scan rate and also provides data storage capability. The sourcemeter was previously calibrated by using a copper foil as a standard. Briefly, 15 mg of each powdered sample was placed in a sample holder of 13 mm diameter between two polished steel pellets that allow pressurizing during the measurements. The samples were pressed at 8 $Ton.cm^{-2}$ with a pneumatic press piston and the electrical conductivity was measured between the top and bottom metallic surface of the press holder at 25 °C. Thickness

of the pressed samples was measured by using a Mitutoyo instrument with an accuracy of ±0.0001 in 2 μm.

The electrical resistivity of the materials was calculated using eq. (1) and using the resistance (*R*) calculated at 1 V with the dimensions of the pressed pellet.

$$\rho = R.a/l \qquad Eq.(1)$$

where *R* is the resistance, *l* the thickness and *a* the area of the circular pellet (13 mm diameter).

Since the electrical conductivity is the reciprocal of the resistivity, it was calculated by taking the inverse of resistivity ($\sigma = 1/\rho$).

For comparison purposes, a commercially available graphene was employed (Graphene nanoplatelets aggregates, sub-micron particles, surface area 300 m^2/g, Strem Chemicals, product 06-0225). The mass employed for the electrical measurements both for the controls and zeolite-based materials was 15 mg.

- Cyclic voltammetry experiments

The electrochemical experiments were performed using a Versastat 3 electrochemical workstation. Two 1 cm^2 AISI-304 stainless steel mesh, mesh number 300 and 0.035 mm wire diameter, coated by drop-casting with a suspension of the material (20 wt. % of active material and 3.6 wt.% polyvynilpyrrolidone in ethanol) was used as electrode (125 μg of active material on each electrode, 250 μg total active material mass). Electrochemical studies were carried out in 300 μL 1 M lithium perchlorate solution in propylene carbonate and using an EL-CELL PAT-CELL commercial electrochemical cell in a 2-electrode configuration with gold current collectors, both electrodes were separated by a 21 mm Whatman™ glass microfibre filter GF/A. The cyclic voltammograms (CVs) were recorded at a scan rate of 50 mV/s. The galvanostatic charge/discharge (GCD) curves for EDLCs were obtained at 2 A/g.

3.- Results

- Synthesis and characterization of Ge-based hybrid composites from Ge-rich zeolites

Ge atoms in tetrahedral coordination within the zeolite frameworks are very labile, particularly for Ge-rich zeolites with Si/Ge ratios below 5.[20-22] While typically considered unfavorable for catalytic

applications, this feature is optimal for creating well-dispersed extra-framework Ge particles for electronic applications, since their size and dispersion can be readily tuned depending on the initial physico-chemical properties of the as-prepared Ge-zeolites and the post-synthetic treatments carried out starting from the as-prepared Ge-zeolites.

We selected ITQ-22 (IWW) [26] and ITQ-33 (ITT),[27-28] for this study because both zeolites can be prepared under identical Ge-rich conditions (as low as Si/Ge~2).[28] In addition, both frameworks feature multipore systems involving interconnected large and medium-pores for IWW (12x10x8-rings, with pore openings of ~6.5x5.0x3.5 Å) and extra-large and medium pores for ITT (18x10x10-rings, with pore openings of ~12.3x5.5x5.5 Å), thereby resulting in similar pore connectivities, but very different framework densities (16.1 and 12.4 T/1000 $Å^3$, respectively) (see Figure 1).

The as-prepared zeolites with Si/Ge = 2 (denoted as IWW-2_a.p. and ITT-2_a.p.) showed the characteristic PXRD patterns of the IWW and ITT topologies, respectively (see Figures 2 and 3). The chemical and elemental analyses of both materials revealed similar Si/Ge molar ratio (~2.5, see Table 1) and organic content (~7-7.5%C and ~1.4-1.6%N), which corresponds to intact hexamethonium molecules trapped within the zeolite crystals during the hydrothermal crystallization process. Scanning electron microcopy (SEM) images showed crystal aggregates formed by stacked thin layers of ~3-4 μm for IWW-2_a.p. (see Figure 4) and arranged needles of ~2-3 μm for ITT-2_a.p (see Figure 5).

Optimal Ge-based hybrid devices require uniform metallic Ge nanoparticles dispersed over a conductive polycyclic aromatic C source, such as graphitic or graphenic species, to favor the electron transport and electrical contact between the Ge nanoparticles. Considering the presence of the occluded organic molecules within the pores of the as-prepared IWW and ITT zeolites, we hypothesized that a simple thermal reduction at high temperature (i.e. 580-700°C), would fullfull both requirements by simultaneoulsy forcing the extraction and aggregation of framework Ge species into well-dispersed metallic nanoparticles and the generation of aromatic C-like entrapped species from ODSA degradation.

To evaluate the most efficient post-synthetic method to form well-defined Ge particles from the above as-prepared materials, we have first focused on the IWW-2 material. The crystalline structure of the IWW-2 zeolite remained almost unaltered when treating it at 580°C with N_2 (see IWW-2_N_2-580°C in Figure 2), while a partial amorphization was observed when treated with N_2 at higher

temperatures (i.e. 700°C, see IWW-2_N_2-700°C in Figure 2). We note that the final organic content in the treated material was only ~1 C wt% (see IWW-2_N_2-580°C and IWW-2_N_2-700°C in Table 2), which is much lower than that in the as-prepared IWW-2 material (~7.8%wt C, see IWW-2_a.p. in Table 2), even though the thermal treatment was performed under non-oxidizing conditions. This observation has also been reported in the literature for other medium and large pore silicates and is attributed to the combination of pore dimensions and the structure of the OSDA used as template.[29]

In order to increase the carbon content in the final materials, we decided to perform the thermal treatments in presence of a light olefin, such as 1-butene, which is known to undergo oligomerization to form carbon deposits within porous materials at these conditions (see experimental section for details).[30-31] As seen in Figure 2, the crystalline structure of the IWW-2 sample was mostly retained after being exposed to 1-butene at 580°C (see IWW-2_$C_4^=$-580°C), but it fully collapsed after being treated with 1-butene at 700°C (see IWW-2_$C_4^=$-700°C). In both cases, we observed a very intense peak centered at 27.5 2θ degrees in their PXRD patterns that corresponds to the formation of metallic germanium particles.[19] Nanoparticle formation was confirmed with FE-SEM, which revealed Ge particles ranging between 50 and 80 nm on the external surface of the composites (see IWW-2_$C_4^=$-580°C and IWW-2_$C_4^=$-700°C in Figure 4), with a significantly higher concentration for the sample treated at 700°C.

Interestingly, a deeper inspection of the IWW-2_$C_4^=$-700°C sample by HR-TEM microscopy revealed a dual Ge distribution, consisting of very small Ge nanoparticles of ~5 nm encapsulated within the silicate particles, and larger Ge nanoparticles of 50-80 nm deposited on the external surface of the silicates (see Figure 6a). The larger Ge nanoparticles presented a Ge@C core-shell structure with a uniform carbon-coating layer 5-10 nm thick (see Figures 6b-c). This carbon overlayer is critical to prevent their undesired agglomeration and oxidation to GeO_2, as well as to minimize the mechanical stress induced by the volume change of Ge in particular applications (i.e. Li ion batteries).[13, 32]

Elemental analysis on the IWW-2_$C_4^=$-700°C sample revealed a carbon content of ~7.7%wt, which is substantially higher than the organic content obtained for the IWW-2 samples treated under inert conditions (~1%wt C, see Table 2). Raman spectra of the carbonaceous species formed in the IWW-2_$C_4^=$-700°C sample showed two well-defined signals centered at ~1580 and 1350 cm^{-1}, which are characteristic features of the sp^2 carbon atoms of graphitic layers (G band) and disordered carbon

or defective graphitic structures (D band), respectively (see IWW-2_C4$_=$-700°C in Figure 7).[33] The higher intensity observed for the G band in the Raman spectrum suggests a large graphitic order degree within the IWW-2_$C_4^=$-700°C sample.

From the previous treatments on the IWW-2 material, one could conclude that the thermal treatment at 700°C in presence of 1-butene allows obtaining a very interesting dual Ge dispersion with relatively high graphitic C content along the entire sample. Thus, we performed the same post-synthetic treatment at 700°C in presence of butene, to evaluate the properties of the ITT-2 zeolite. Akin to IWW-2, the crystalline structure of ITT-2 material also collapsed and its PXRD pattern featured an intense peak centered at 27.5 2θ degrees indicating the formation of metallic Ge particles (see PXRD pattern for ITT-2_$C_4^=$-700°C in Figure 3). FE-SEM and HR-TEM images show the formation of larger Ge particles than those observed before for IWW-2, with average sizes ranging between 80 and 120 nm (see ITT-2_$C_4^=$-700°C in Figures 5 and 8). It could be envisioned that the combination of larger pores and lower framework density in the ITT zeolite (~12 Å and 12.4 T/1000 Å^3) would offer fewer diffusional restrictions for the extra-framework Ge atoms to move and agglomerate once extracted from the zeolite framework compared to IWW zeolite (~6.5 Å and 16.1 T/1000 Å^3). However, the different distribution of the secondary building units (SBUs) that preferentially host Ge atoms (i.e. D4Rs and 3-rings) along the ITT and IWW frameworks could also present an important influence on the achieved Ge nanoparticles. It is important to note that the extra-large pore ITT zeolite presents almost equally distributed D4Rs along the entire framework, whereas the IWW zeolite contains exclusively these D4Rs in the interlayer region of high-silica layers. Further, the more open pore topology of the ITT zeolite favors olefin oligomerization reactions, resulting in a remarkably larger C contents (~23%wt C, see ITT-2_$C_4^=$-700°C in Table 2) compared to the treated IWW-2 sample.

Given that cost is a very important issue when designing Ge-based hybrid materials for electronic devices, we have investigated the use of IWW precursors presenting half of the Ge content (Si/Ge~4, IWW-4, see synthesis details in the experimental section). Although a decrease in Ge content could negatively impact the conductivity properties, we reasoned that a better dispersion along the IWW framework could result in an improved uniformity after the heat treatment, ultimately enhancing electronic conduction. The as-prepared IWW-4 material showed the characteristic PXRD pattern of the IWW framework (see IWW-4_a.p. in Figure 3), and, similar to IWW-2, the crystals were also mainly formed by stacked thin layers of ~4 μm (see FE-SEM images for IWW-4_a.p. in Figure 5). After

treating the IWW-4_a.p. material at 700°C in presence of 1-butene, the initial crystalline framework collapsed and revealed the peak at 27.5 2θ degrees associated with metallic Ge species (see IWW-4_$C_4^=$-700°C in Figure 3). HR-TEM images showed the formation of homogenous Ge@C particles with average sizes between 30-60 nm (see FE-SEM and HR-TEM images in Figures 5 and 8), together with the presence of very small trapped Ge nanoparticles of ~5 nm within silicate particles (see Figure 8).

- Conductivity performance

We surmised that the synergy between large and small metallic Ge nanoparticles dispersed in a conductive graphitic matrix would induce remarkable conducting properties to the final material, even if the original crystalline structure of the zeolite was not maintained. As seen in Table 2, the measured electrical conductivities at a given voltage (1 V) clearly show an influence of the post-synthetic treatments. Unsurprisingly, the as-prepared Ge-containing zeolites behaved as insulators rather than conductors (0.1-0.3 MΩ·m), with negligible measured conductivity values (see IWW-2_a.p., ITT-2_a.p. and IWW-4_a.p. in Table 2), given that isolated Ge species in the zeolite frameworks together with the occlusion of non-aromatic organic molecules within the zeolite pores should not conduct charge. The resistivity values for the Ge-containing zeolites after being treated at 580°C (either in N_2 and 1-butene) are remarkably lower compared to the as-prepared materials (<5 MΩ·m, see IWW-2_N_2-580°C and IWW-2_$C_4^=$-580°C in Table 2), but their conductivity values still remained pretty low (< 1E-05 S/m, see IWW-2_N_2-580°C and IWW-2_$C_4^=$-580°C in Table 2). The slight improvement in their electrical conductivity could be ascribed to the presence of some aromatic-based C species (~1-2 C wt%) after the thermal treatments at 580°C.

In contrast, the measured conductivities on the samples treated at 700°C, in particular those treated in presence of 1-butene, are substantially higher, achieving values of 1-3 S/m (see IWW-2_$C_4^=$-700°C, ITT-2_$C_4^=$-700°C and IWW-4_$C_4^=$-700°C in Table 2), which are comparable to well-stablished electrical conductors, such as commercially available graphene (~3 S/m, see Table 2). In fact, significant differences can be observed when comparing the electrical conductivity profiles for the same Ge-containing sample, IWW-2, after being treated at 700°C, but under different atmospheres (N_2 or 1-butene). As seen in Figure 9, the I/V plot for the IWW-2 material treated at 700°C with butene performs as an outstanding conductor material, whereas the IWW-2 material treated at 700°C with N_2 mostly performs as an insulator material. However, and despite its low conductivity,

a deeper inspection of the I/V curve for the IWW-2_N_2-700°C revealed a semiconductor-type behavior, where the presence of two well-defined regimes indicate the performance of a resistor at low voltages and, at least partially, the performance of a conductor material at high voltages. Similar semiconductor behaviors have been described for other metal-containing zeolites, such as Co-FAU.[34] We hypothesize that a better metallic Ge nanoparticle dispersion along the sample combined with the higher graphitic C content, is responsible for the higher conductivity measured for the IWW-2_$C_4^=$-700°C compared to the one of IWW-2_N_2-700°C.

In order to unravel the influence of these two parameters, we compared the electronic behavior of the other two Ge-containing materials, ITT-2 and IWW-4, after being treated with 1-butene at 700°C. As seen in Figure 10, the ITT-2_$C_4^=$-700°C also performed as an excellent conductor material, but its I/V profile presented lower current intensities at a given voltage than IWW-2_$C_4^=$-700°C, despite the remarkably higher aromatic C content within the treated ITT-2 material (22.9 and 7.6%wt C for ITT-2_$C_4^=$-700°C and IWW-2_$C_4^=$-700°C, respectively, see Table 2). This result clearly indicates that the better Ge dispersion along the Ge-based hybrid material has a stronger influence on the electronic properties of the Ge-composite than graphitic C content. This conclusion is further supported by the very similar I/V profile results obtained with the sample prepared with much less Ge content, IWW-4, compared to the Ge-rich IWW-2 sample after being treated with 1-butene at 700°C (see IWW-2_$C_4^=$-700°C and IWW-4_$C_4^=$-700°C in Figure 10). The enhanced Ge dispersion in IWW-4_$C_4^=$-700°C that was observed by microscopy (see Figures 5-bottom and 8-bottom), is consistent with the high conductivity values even when containing only half of the Ge. Notably, this sample maintained virtually identical conductivity profiles even after six months of being treated and stored under ambient conditions, thus revealing an outstanding stability. Based on these experimental observations, the ability to maximize and control the dispersion of the Ge-particles within the nanometer scale along the Ge-composites is currently a main research topic in our laboratories to improve their conductivity performances.

For comparison purposes, a medium-pore Ge-free Silicalite-1 material (MFI structure) was synthesized to evaluate its conductivity behavior after being treated with 1-butene at 700°C (see synthesis details in the experimental section and PXRD pattern in Figure 11). This sample had a C content of ~7%wt, predominantly in the form of graphitic species with high order degree, as revealed by Raman spectroscopy (see Figure 7). However, this material showed a considerably lower conductivity compared to the treated Ge-containing zeolites (see Figure 10), further demonstrating

the necessity of having well-dispersed metallic Ge nanoparticles to obtain efficient conductor materials.

In addition, two Ge-based graphene materials have been prepared also for comparison purposes. On the one hand, we have prepared a Ge-SiO_2/Graphene, with a similar chemical composition to the IWW-4_$C_4^=$-700°C sample (21.4%wt GeO_2, 65.7%wt SiO_2, and 12.9 %wt Graphene, see experimental section for details). This Ge-SiO_2/Graphene sample gives a conductivity value of ~2.87E-03 S/m, which is substantially lower than the measured for the IWW-4_$C_4^=$-700°C (~1.9 S/m, see Table 2). On the other hand, we have also prepared a Ge/Graphene sample containing an overall Ge content similar to the one present in the IWW-4_$C_4^=$-700°C, but without including SiO_2 in the formulation (21.4%wt GeO_2, and 78.6%wt Graphene, see experimental section for details). This Ge/Graphene sample gives a conductivity value of ~0.94 S/m, which is lower than the values measured for the pure Graphene (~2.98 S/m) and for the IWW-4_$C_4^=$-700°C sample (~1.90 S/m) (see Table 2). These results put in relevance the importance of the initial Ge-rich zeolite precursor to properly allow the formation of Ge-composites with unique physico-chemical properties, and, consequently, improved conductivity performances.

As a preliminary study to evaluate the reversible capacity and cycling capability in a battery cell of these Ge-composites, the IWW-4_$C_4^=$-700°C sample has been studied as electrode in electrochemical double layer capacitors (EDLCs). In this regard, the electrochemical performance of the material has been studied by cyclic voltammetry at room temperature, using 1M lithium perchlorate in propylene carbonate as electrolyte. As seen in Figure 12, the shape of the curves is similar after 30 cycles and only a slight change in the current is observed, indicating good stability of the material for their application in electrochemical energy storage devices.

4.- Conclusions

We subjected two different Ge-rich zeolites, ITQ-22 (IWW) and ITQ-33 (ITT) to post-synthetic treatments at different temperatures (580 and 700°C) and controlled atmospheres (N_2 and 1-butene) and studied their conductivity behavior. The resulting Ge-based hybrid composites were analyzed by different techniques to reveal the nature, size, dispersion and stability of the metallic Ge nanoparticles in the final structure. The dispersion of metallic Ge nanoparticles was influenced by the post-synthetic thermal treatment, the pore topology of the parent zeolite, and the initial Si/Ge molar ratio. We showed that the IWW zeolite with an initial Si/Ge molar ratio of ~4, featured

electrical conductivity performance commensurate to that of graphene after being treated with 1-butene at 700°C. The post-synthetic treatment of Ge-based zeolite precursors opens an interesting research pathway to design efficient Ge-based hybrid composites, which could have important implications in the preparation of electrodes for lithium-ion batteries.

Acknowledgements

This work has been supported by the Spanish Government-MINECO through ‘‘Severo Ochoa” (SEV-2016-0683) and RTI2018-101033-B-I00, and by La Caixa Foundation through MIT-SPAIN SEED FUND (LCF/PR/MIT17/11820002). A.R.F. acknowledges the Spanish Government-MINECO for a FPU scholarship (FPU2017/01521). The Electron Microscopy Service of the UPV is acknowledged for their help in sample characterization. We thank Javier van Herpt for the cyclic voltammetry experiment.

Figure 1: Framework structures of the IWW (left) and ITT (right)

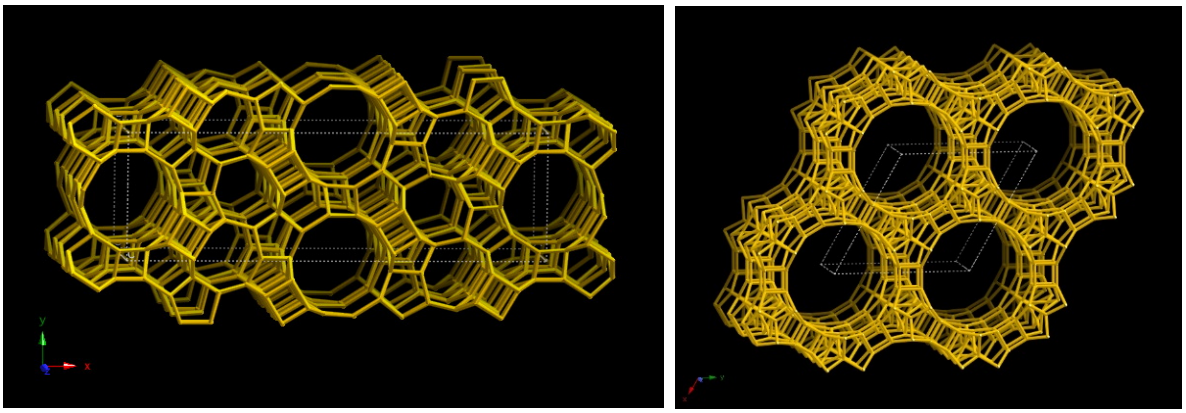

Figure 2: PXRD patterns of the Ge-rich IWW-2 zeolite (Si/Ge~2) after different post-synthetic treatments

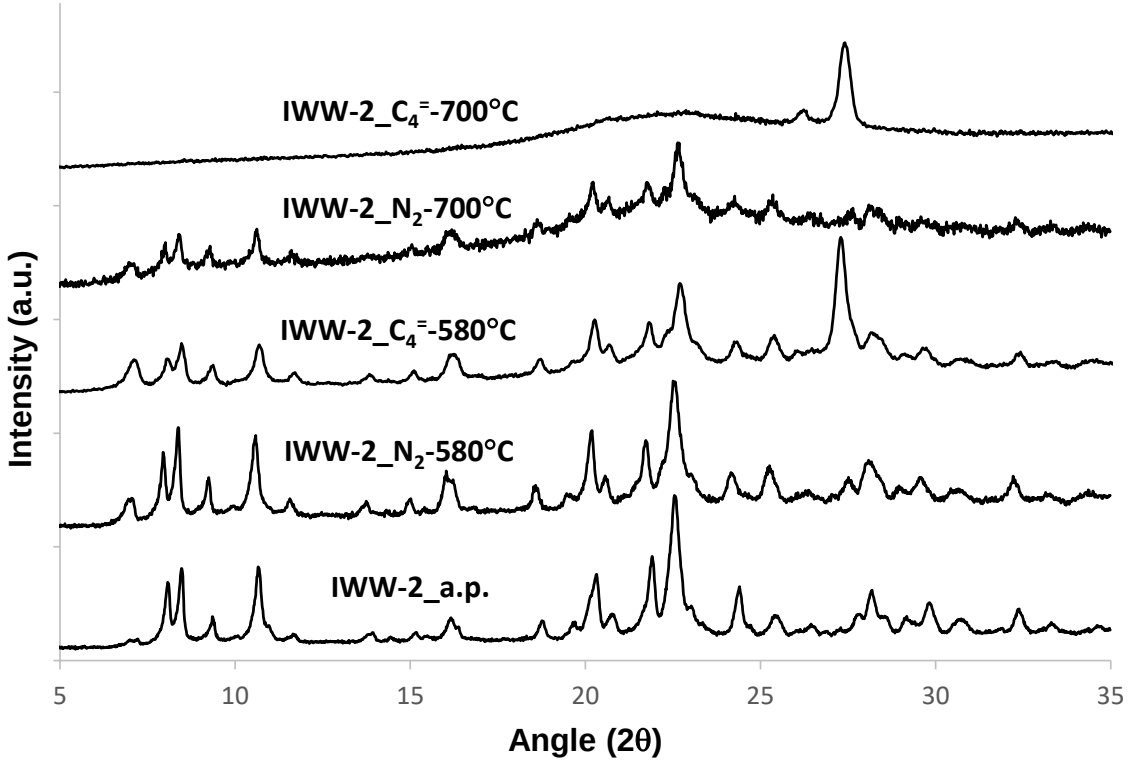

Figure 3: PXRD patterns of the Ge-containing IWW-4 (Si/Ge~4) and ITT-2 (Si/Ge~2) zeolites in their as-prepared forms and after being post-synthetically treated with butene at 700°C

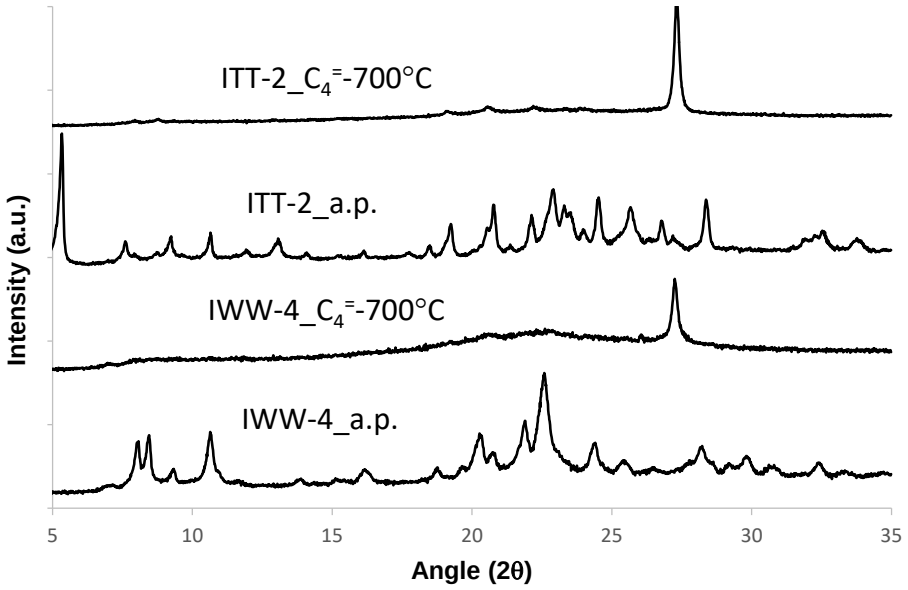

Figure 4: FE-SEM images of the Ge-rich IWW-2 zeolite (Si/Ge~2) after different post-synthetic treatments

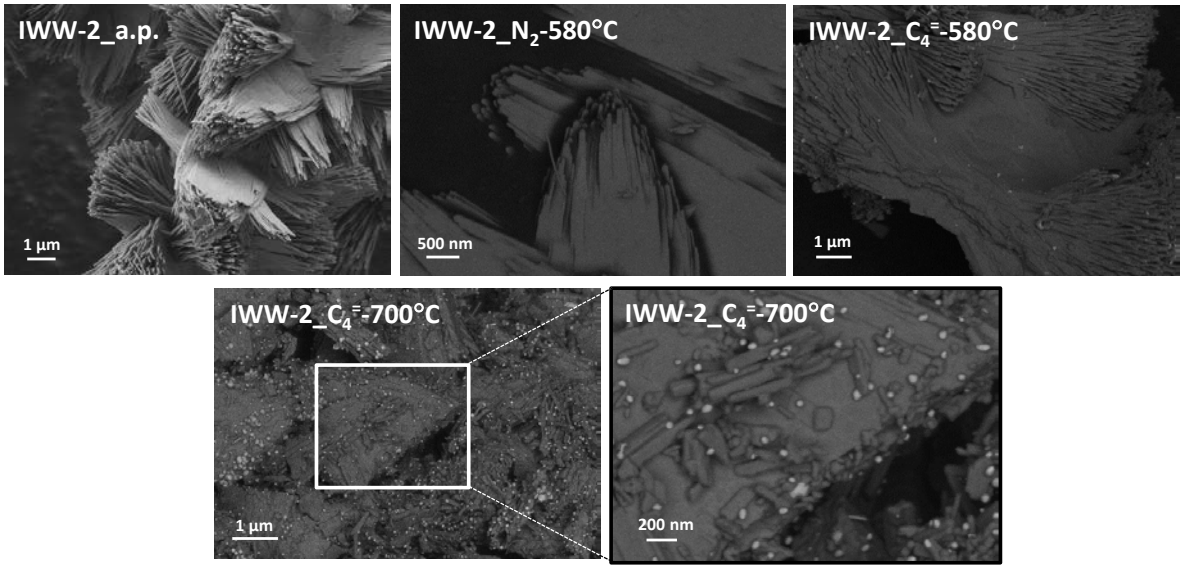

Figure 5: FE-SEM images of the Ge-containing IWW-4 (Si/Ge~4) and ITT-2 (Si/Ge~2) zeolites in their as-prepared forms and after being post-synthetically treated with butene at 700°C

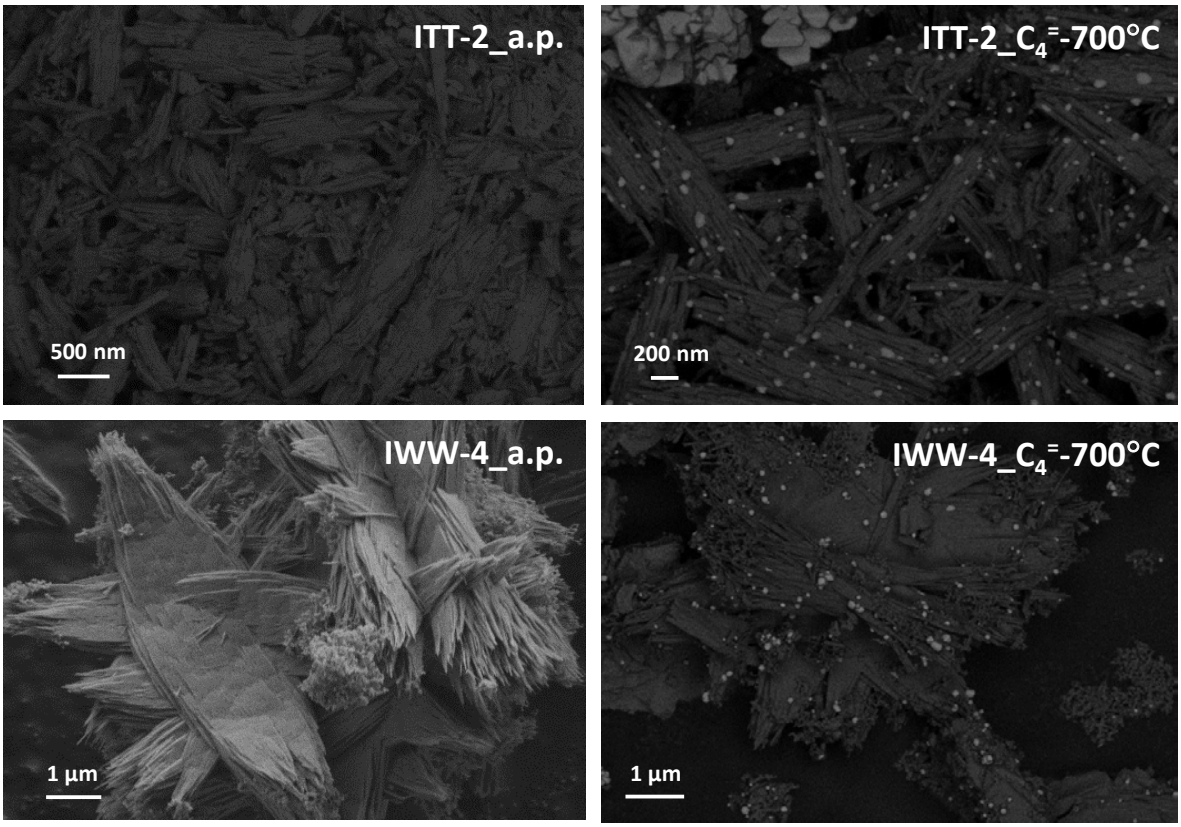

Figure 6: STEM (a) and HR-TEM images (b, c) for the IWW-2_$C_4^=$-700°C

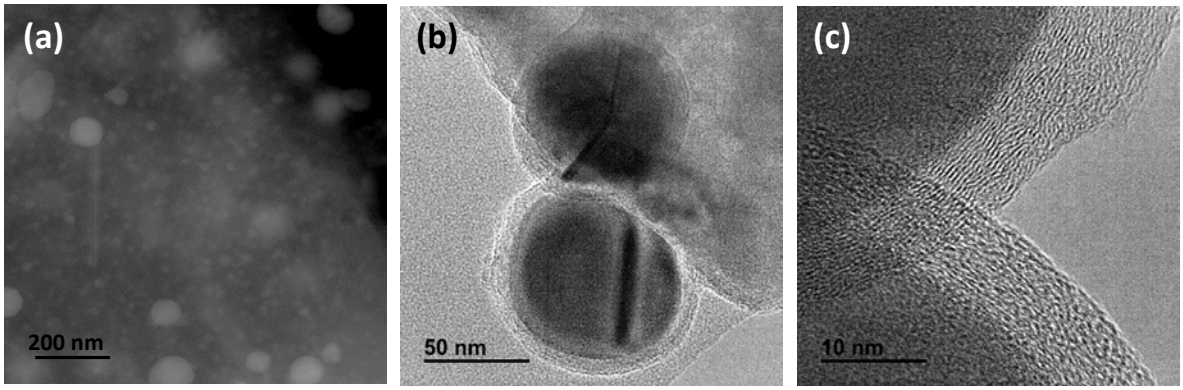

Figure 7: Raman spectrum of the Ge-based and pure silica MFI hybrid composites after being treated with butene at 700°C

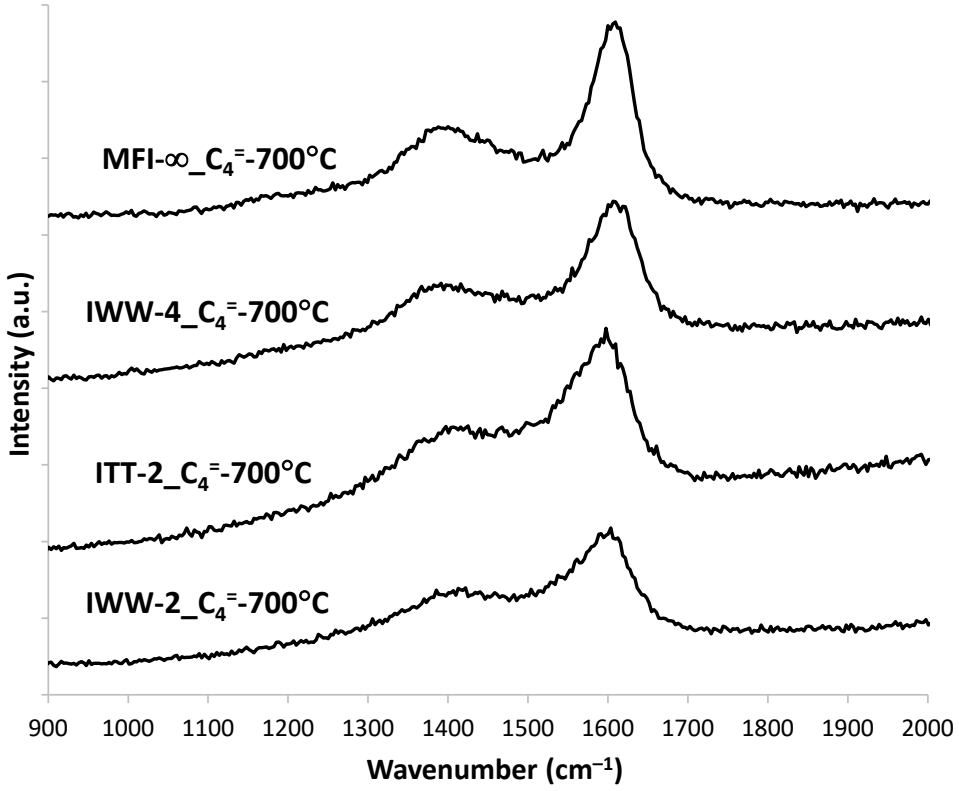

Figure 8: STEM and HR-TEM images of the Ge-containing ITT-2 (Si/Ge~2) and IWW-4 (Si/Ge~4) zeolites after being post-synthetically treated with butene at 700°C

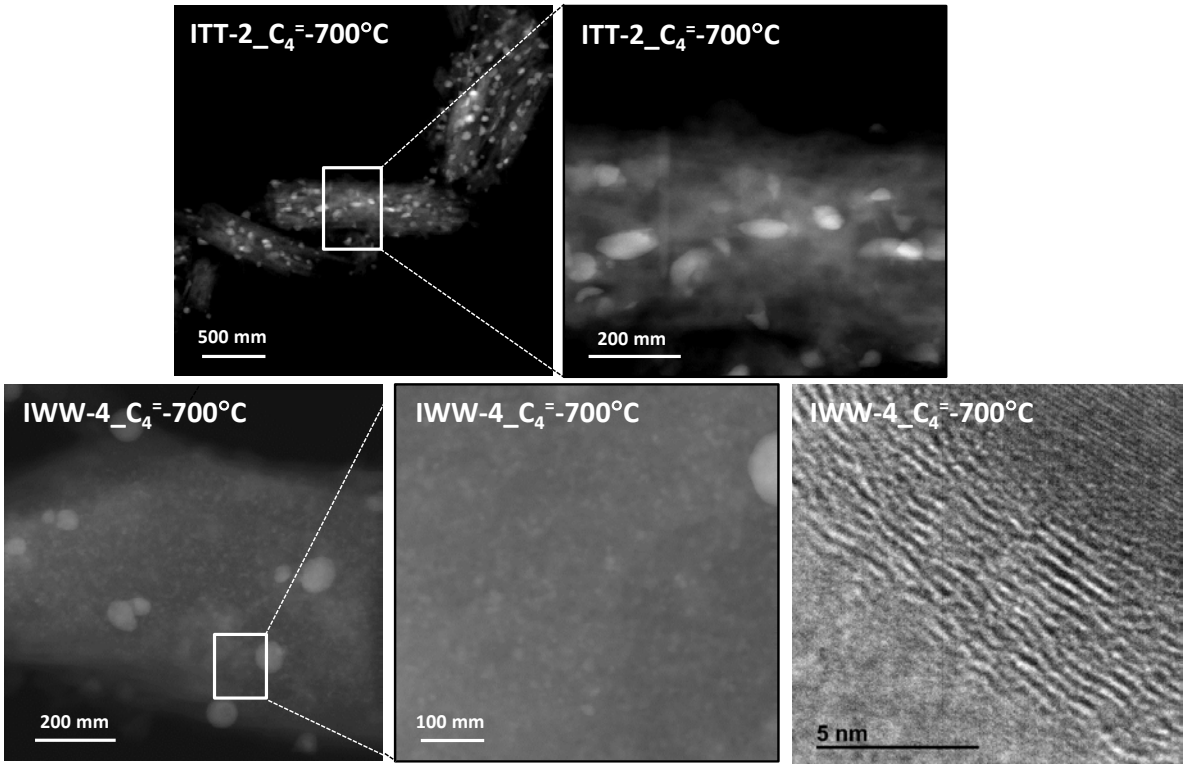

Figure 9: I-V plot comparing the electrical conductivity of the Ge-rich IWW-2 zeolite (Si/Ge~2) after being treated with N_2 or butene at 700°C

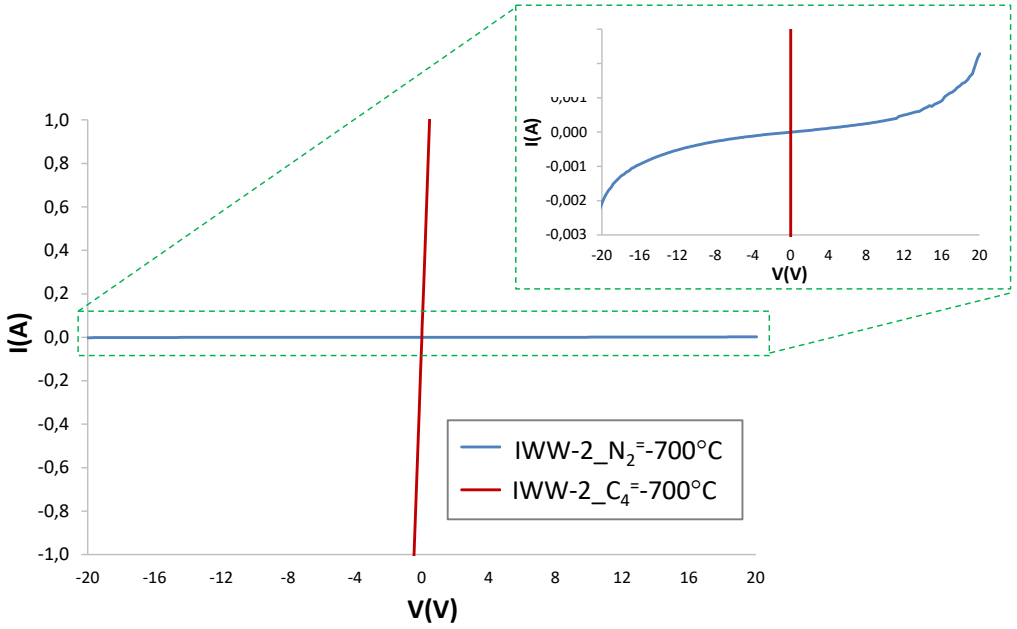

Figure 10: I-V plot comparing the electrical conductivity of the different Ge-based hybrid composites and pure silica MFI after being treated with butene at 700°C

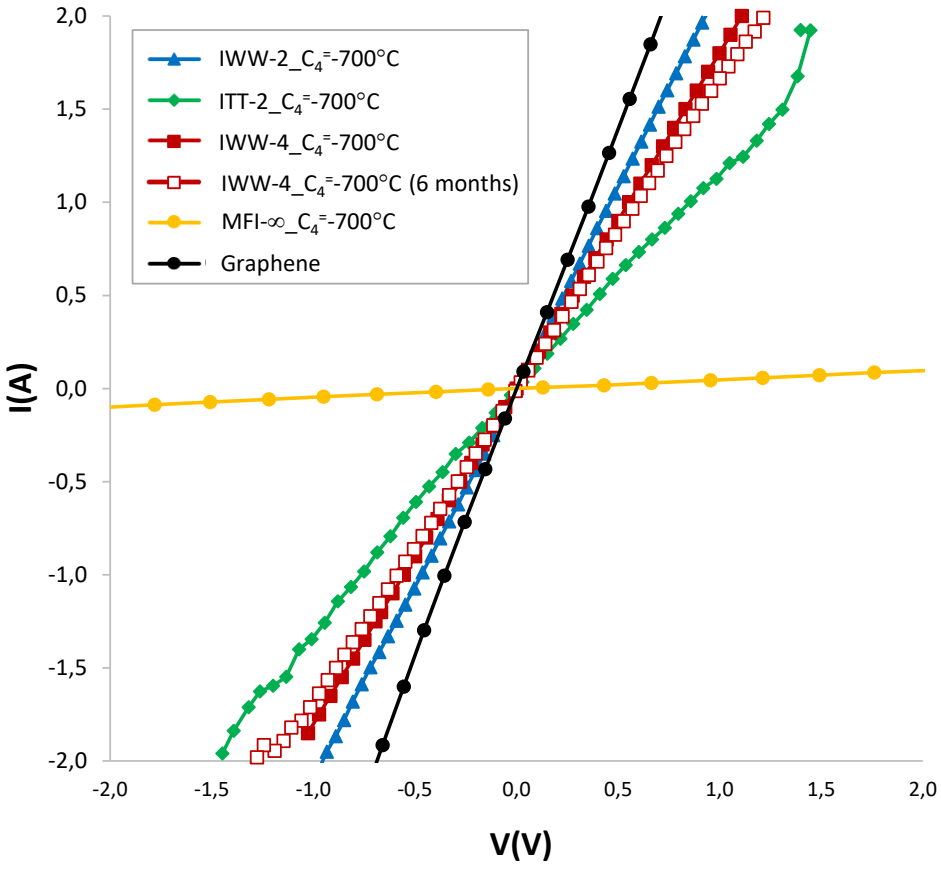

Figure 11: PXRD pattern (A) and FE-SEM image (B) of the silicalite zeolite (MFI) after being treated with butene at 700°C

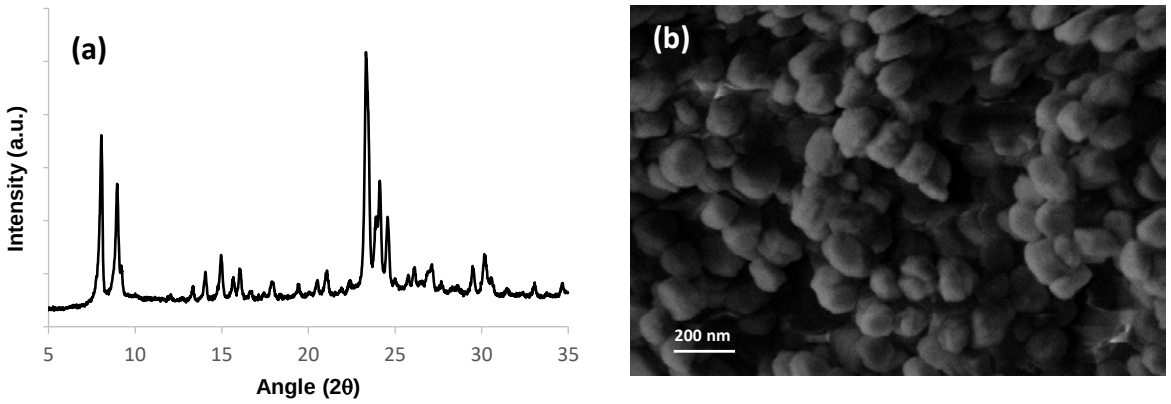

Figure 12. (A) Cyclic voltammetry curves at a scan rate of 50 mV/s during 30 cycles, (B) Galvanostatic charge/discharge curves at 2.0 A/g.

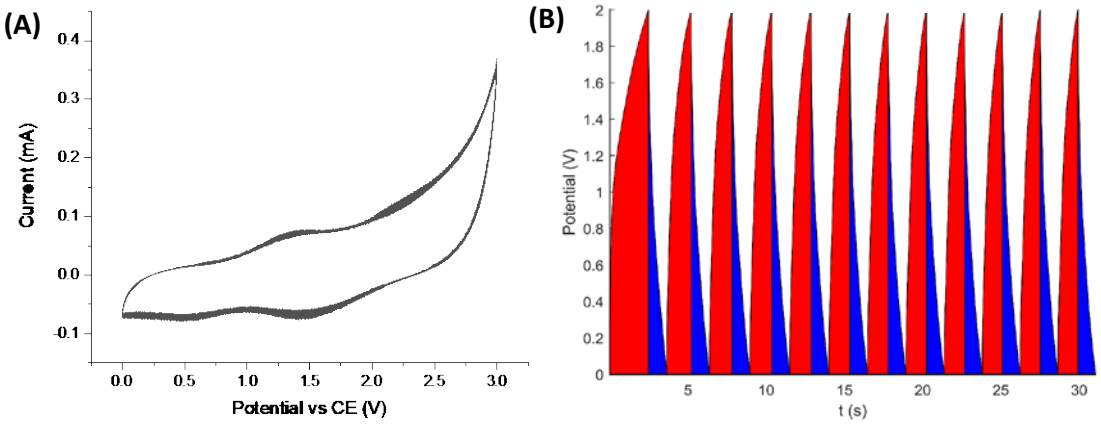

Table 1: Chemical and elemental analyses of the as-prepared zeolites

Zeolite	Si/Ge	%wt N	%wt C
IWW-2	2.5	1.58	7.76
ITT-2	2.4	1.37	6.64
IWW-4	5.2	1.42	7.04
MFI	∞	0.63	6.52

Table 2: Elemental analyses and electrical conductivity data (measured at a voltage of 1 V) obtained from post-synthetically treated zeolites.

Zeolite	%wt N	%wt C	Resistivity (Ω·m)	Conductivity (S/m)
IWW-2_a.p.	1.58	7.76	1.49E+05	6.72E-06
IWW-2_N_2-580°C	0.00	0.93	5.15E+04	1.94E-05
IWW-2_$C_4^=$-580°C	0.00	1.72	1.11E+06	9.04E-07
IWW-2_N_2-700°C	0.00	1.35	1.08E+03	9.25E-04
IWW-2_$C_4^=$-700°C	0.00	7.65	0.45	2.24
ITT-2_a.p.	1.37	6.64	∞	0.00
ITT-2_$C_4^=$-700°C	0.00	22.94	0.81	1.23
IWW-4_a.p.	1.42	7.04	3.50E+05	2.85E-06
IWW-4_$C_4^=$-700°C	0.00	12.95	0.53	1.90
IWW-4_$C_4^=$-700°C (6 months)	0.00	12.95	0.56	1.77
MFI-∞_$C_4^=$-700°C	0.00	6.65	3.17	0.32
Graphene	---	---	0.34	2.98
Ge/Graphene	---	---	1.06	0.94
Ge-SiO_2/Graphene	---	---	348.4	2.87E-03

References:

1. *Handbook of Advanced Electronic and Photonic Materials and Devices. Nalwa, H. (Ed)*. Academic Press: 2000.
2. Liu, C.; Li, F.; Ma, L. P.; Cheng, H. M., Advanced Materials for Energy Storage. *Adv. Mater.* **2010,** *22*, E28-E62.
3. Wang, D.; Chang, Y. L.; Wang, Q.; Cao, J.; Farmer, D. B.; Gordon, R. G.; Dai, H., Surface Chemistry and Electrical Properties of Germanium Nanowires. *J. Am. Chem. Soc.* **2004,** *126*, 11602-11611.
4. Kennedy, T.; Mullane, E.; Geaney, H.; Osiak, M.; O'Dwyer, C.; Ryan, K. M., High-Performance Germanium Nanowire-Based Lithium-Ion Battery Anodes Extending over 1000 Cycles Through in Situ Formation of a Continuous Porous Network. *Nano. Lett.* **2014,** *14*, 716-723.
5. Wang, D.; Chang, Y. L.; Liu, Z.; Dai, H., Oxidation Resistant Germanium Nanowires: Bulk Synthesis, Long Chain Alkanethiol Functionalization, and Langmuir-Blodgett Assembly. *J. Am. Chem. Soc.* **2005,** *127*, 11871-11875.
6. Tabet, N.; Al-Sadah, J.; Salim, M., Growth of oxide layer on germanium (011) substrate under dry and wet atmospheres. *Surf. Rev. Lett.* **1999,** *6*, 1053-1060.
7. Cui, G.; Gu, L.; Zhi, L. J.; Kaskhedikar, N.; van Aken, P. A.; Müllen, K.; Maier, J., A Germanium–Carbon Nanocomposite Material for Lithium Batteries. *Adv. Mater.* **2008,** *20*, 3079-3083.
8. Li, W.; Yang, Z.; Cheng, J.; Zhong, X.; Gu, L.; Yu, Y., Germanium nanoparticles encapsulated in flexible carbon nanofibers as self-supported electrodes for high performance lithium-ion batteries. *Nanoscale* **2014,** *6*, 4532-4537.
9. Seo, M. H.; Park, M.; Lee, K. T.; Kim, K.; Kim, J.; Cho, J., High performance Ge nanowire anode sheathed with carbon for lithium rechargeable batteries. *Energy Environ. Sci.* **2011,** *4*, 425-428.
10. Hwang, I. S.; Kim, J. C.; Seo, S. D.; Lee, S.; Lee, J. H.; Kim, D. W., A binder-free Ge-nanoparticle anode assembled on multiwalled carbon nanotube networks for Li-ion batteries. *Chem. Commun.* **2012,** *48*, 7061-7063.
11. Cui, G.; Gu, L.; Kaskhedikar, N.; van Aken, P. A.; Maier, J., A novel germanium/carbon nanotubes nanocomposite for lithium storage material. *Electrochim. Acta* **2010,** *55*, 985-988.
12. DiLeo, R. A.; Frisco, S.; Ganter, M. J.; Rogers, R. E.; Raffaelle, R. P.; Landi, B. J., Hybrid Germanium Nanoparticle–Single-Wall Carbon Nanotube Free-Standing Anodes for Lithium Ion Batteries. *J. Phys. Chem. C* **2011,** *115*, 22609-22614.
13. Xue, D. J.; Xin, S.; Yan, Y.; Jiang, K. C.; Yin, Y. X.; Guo, Y. G.; Wan, L. J., Improving the Electrode Performance of Ge through Ge@C Core−Shell Nanoparticles and Graphene Networks. *J. Am. Chem. Soc.* **2012,** *134*, 2512-2515.
14. Yang, C.; Jiang, Y.; Liu, X.; Zhonga, X.; Yu, Y., Germanium encapsulated in sulfur and nitrogen co-doped 3D porous carbon as an ultra-long-cycle life anode for lithium ion batteries. *J Mater. Chem. A* **2016,** *4*, 18711-18716.
15. Mo, R.; Rooney, D.; Sun, K.; Yang, H. Y., 3D nitrogen-doped graphene foam with encapsulated germanium/nitrogen-doped graphene yolk-shell nanoarchitecture for high-performance flexible Li-ion battery. *Nature Commun.* **2017,** *8*, Article number: 13949.
16. Mathur, S.; Shen, H.; Donia, N.; Rügamer, T.; Sivakov, V.; Werner, U., One-Step Chemical Vapor Growth of Ge/SiCxNy Nanocables. *J. Am. Chem. Soc.* **2007,** *129*, 9746-9752.
17. Yang, S.; Feng, X.; Ivanovici, S.; Müllen, K., Fabrication of Graphene-Encapsulated Oxide Nanoparticles: Towards High-Performance Anode Materials for Lithium Storage. *Angew. Chem., Int. Ed.* **2010,** *49*, 8408-8411.

18. Yu, Y.; Gu, L.; Wang, C.; Dhanabalan, A.; van Aken Priv.-Doz, P. A.; Maier, J., Encapsulation of Sn@carbon Nanoparticles in Bamboo-like Hollow Carbon Nanofibers as an Anode Material in Lithium-Based Batteries. *Angew. Chem., Int. Ed.* **2009,** *48*, 6485-6489.
19. Ren, J. G.; Wu, Q. H.; Tang, H.; Hong, G.; Zhang, W.; Lee, S. H., Germanium–graphene composite anode for highenergy lithium batteries with long cycle life. *J. Mater. Chem. A* **2013,** *1*, 1821-1826.
20. Jiang, J.; Yu, J.; Corma, A., Extra-Large-Pore Zeolites: Bridging the Gap between Micro and Mesoporous Structures. *Angew. Chem., Int. Ed.* **2010,** *49*, 3120-3145.
21. Rodríguez-Fernández, A.; Llopis, F. J.; Martínez, C.; Moliner, M.; Corma, A., Increasing the stability of the Ge-containing extra-large pore ITQ-33 zeolite by post-synthetic acid treatments. *Micropor. Mesopor. Mater.* **2018,** *267*, 35-42.
22. Eliášová, P.; Opanasenko, M.; Wheatley, P. S.; Shamzhy, M.; Mazur, M.; Nachtigall, P.; Roth, W. J.; Morris, R. E.; Čejka, J., The ADOR mechanism for the synthesis of new zeolites. *Chem. Soc. Rev.* **2015,** *44*, 7177-7206.
23. Davis, M. E.; Lobo, R. F., Zeolite and molecular sieve synthesis. *Chem. Mater.* **1992,** *4*, 756-768.
24. Moliner, M.; Rey, F.; Corma, A., Towards the Rational Design of Efficient Organic Structure-Directing Agents for Zeolite Synthesis. *Angew. Chem., Int. Ed.* **2013,** *52*, 13880-13889.
25. Kim, K.; Lee, T.; Kwon, Y.; Seo, Y.; Song, J.; Park, J. K.; Lee, H.; Park, J. Y.; Ihee, H.; Cho, S. J.; Ryoo, R., Lanthanum-catalysed synthesis of microporous 3D graphene-like carbons in a zeolite template. *Nature* **2016,** *535*, 131-135.
26. Corma, A.; Rey, F.; Valencia, S.; Jordá, J. L.; Rius, J., A zeolite with interconnected 8-, 10- and 12-ring pores and its unique catalytic selectivity. *Nat. Mat.* **2003,** *2*, 493-497.
27. Corma, A.; Díaz-Cabañas, M. J.; Jordá, J. L.; Martínez, C.; Moliner, M., High-throughput synthesis and catalytic properties of a molecular sieve with 18- and 10-member rings. *Nature* **2006,** *443*, 842–845.
28. Moliner, M.; Díaz-Cabañas, M. J.; Fornés, V.; Martínez, C.; Corma, A., Synthesis methodology, stability, acidity, and catalytic behavior of the member ring pores ITQ-33 zeolite. *J. Catal.* **2008,** *254*, 101-109.
29. Baldoví, H. G.; Valencia, S.; Alvaro, M.; Asiri, A. M.; García, H., Highly fluorescent C-dots obtained by pyrolysis of quaternary ammonium ions trapped in all-silica ITQ-29 zeolite. *Nanoscale* **2015,** *7*, 1744-1752.
30. Lu, H.; Kim, K.; Kwon, Y.; Sun, X.; Ryoo, R.; Zhao, X. S., Zeolite-templated nanoporous carbon for high-performance supercapacitors. *J. Mater. Chem. A* **2018,** *6*, 10388-10394.
31. Díaz-Rey, M. R.; Paris, C.; Martínez-Franco, R.; Moliner, M.; Martínez, C.; Corma, A., Efficient Oligomerization of Pentene into Liquid Fuels on Nanocrystalline Beta Zeolites. *ACS Catal.* **2017,** *7*, 6170-6178.
32. Ng, S. H.; Wang, J.; Wexler, D.; Konstantinov, K.; Guo, Z. P.; Liu, H. K., Highly Reversible Lithium Storage in Spheroidal Carbon-Coated Silicon Nanocomposites as Anodes for Lithium-Ion Batteries. *Angew. Chem., Int. Ed.* **2006,** *45*, 6896-6899.
33. Wu, J. B.; Lin, M. L.; Cong, X.; Liu, H. N.; Tan, P. H., Raman spectroscopy of graphene-based materials and its applications in related devices. *Chem. Soc. Rev.* **2018,** *47*, 1822-1873.
34. Alvaro, M.; Cabeza, J. F.; Fabuel, D.; García, H.; Guijarro, E.; Martínez de Juan, J. L., Electrical conductivity of zeolite films: Influence of charge balancing cations and crystal structure. *Chem. Mater.* **2006,** *18*, 26-33.

Table of Contents (TOC)